

The Far Ultraviolet Spectroscopic Explorer: Mission Overview and Prospects for Studies of the Interstellar Medium and High Velocity Clouds

Kenneth R. Sembach

*Department of Physics & Astronomy, The Johns Hopkins University,
Baltimore, MD 21218, U.S.A*

Abstract. The *Far Ultraviolet Spectroscopic Explorer* (FUSE) is a NASA astronomy mission that will explore the 905–1187Å wavelength region at high spectral resolution. Funded by NASA’s Explorer Program, this *Origins* mission is scheduled for a 1999 launch and at least three years of operations. The development of FUSE is being led by the Johns Hopkins University, with major contributions to the program from the University of Colorado, the University of California-Berkeley, the space agencies of Canada and France, and corporate partners.

FUSE will have approximately 10,000 times the sensitivity of its pioneering predecessor, *Copernicus*, which operated in the 1970s. Much of the FUSE Science Team observing time will be dedicated to studying the interstellar medium of the Milky Way and Magellanic Clouds. Observations of high velocity clouds play an important role in the FUSE program. In this paper, I outline some of the FUSE Science Team plans for observing HVCs. Simple absorption line models are also provided for investigators seeking to identify atomic and molecular species in this wavelength region.

1. Introduction

With the launch of the *Far Ultraviolet Spectroscopic Explorer* (FUSE) in 1999, the astronomical community will have access to the first long duration satellite devoted to high-resolution ($\lambda/\Delta\lambda \approx 24,000\text{--}30,000$) spectroscopic studies of the far ultraviolet (far-UV) universe since the *Copernicus* mission. FUSE will have a point source sensitivity approximately 10,000 times that of *Copernicus*, which will allow systematic studies of distant regions in the Milky Way and other galaxies to be conducted at high spectral resolution in the 905–1187 Å bandpass for the first time. FUSE will also be able to observe the far-UV light from distant quasars and active galactic nuclei.

The far-UV wavelength region is rich in spectral line diagnostics of plasmas ranging in temperature from $10^1\text{--}10^6$ K. It encompasses the Lyman series of H I and D I, as well as resonance lines of the heavy element species C I, C II, C III, N I, N II, N III, O I, O VI, F I, Mg II, Al II, Si II, P III, P IV, P V, S III, S IV, S VI, Cl I, Cl II, Ar I, Ar II, Fe II, and Fe III. Weak lines of other heavy elements (e.g., Cr, Mn, Ni) and low excitation fine-structure lines of C I, C II, N I, and N II may

be visible along some sight lines. The bandpass also contains molecular lines in the Lyman and Werner systems of H_2 and HD, and the $B^1\Sigma_u^+ - X^1\Sigma_g^+$ and $C^1\Sigma_u^+ - X^1\Sigma_g^+$ bands of CO.

2. FUSE Team Science Investigations

During the first three years of operation, approximately half of the FUSE observing time will be used by Guest Investigators selected through a competitive peer-reviewed process, which at the time of writing has been completed for the first observing cycle. A small amount (roughly 10%) of the total observing time has also been reserved for the French and Canadian astronomical communities. The remainder will be used by the FUSE Science Team, which will undertake several large science investigations as well as a number of moderate-sized programs designed to study specific astronomical objects or phenomena. The two primary science programs include:

- 1) A study of the D/H ratio and its dependence upon the chemical evolution of the interstellar gas in the Milky Way and intergalactic gas in the low redshift universe.
- 2) A study of the origins and properties of hot ($T \sim 10^5\text{--}10^6$ K) interstellar gas in the Milky Way and Magellanic Clouds as traced through O VI absorption and emission.

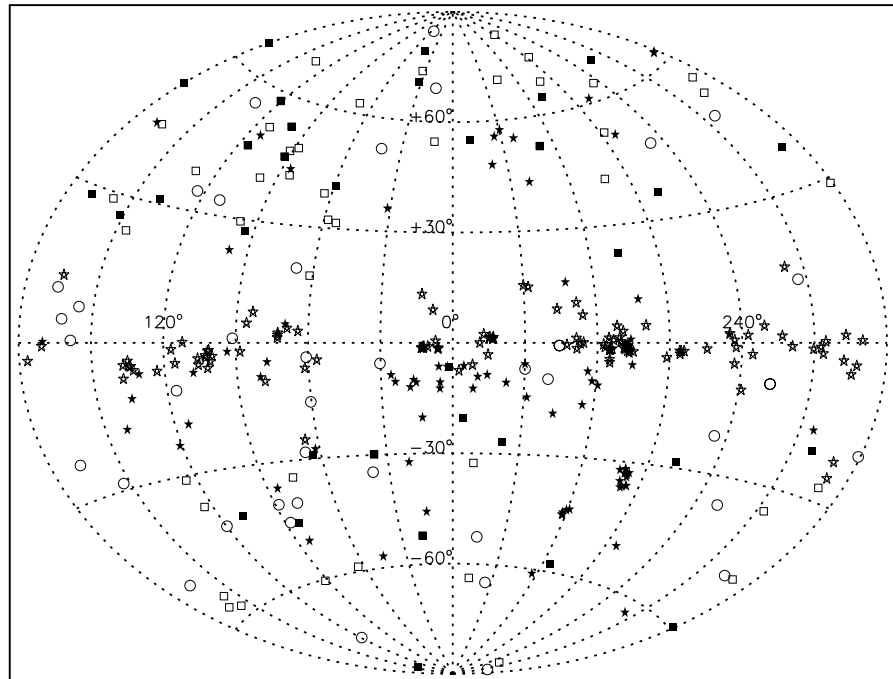


Figure 1. Aitoff projection of the FUSE Team O VI and D/H program sight lines in Galactic coordinates. The Galactic center is at the center of the figure. *Open circles*: Local ISM ($d < 300$ pc); *Open stars*: Galactic disk ($|z| < 300$ pc); *Filled stars*: Galactic halo ($|z| > 300$ pc); *Filled squares*: O VI and D/H extragalactic; *Open squares*: D/H extragalactic snapshots.

To conduct these two comprehensive studies, the FUSE Science Team will observe a large number of objects in the Galactic disk and halo. Figure 1 is a projection of these sight lines onto the sky. The sight lines sample the interstellar medium (ISM) in a variety of directions over distances ranging from a few parsecs to tens of kiloparsecs. The types of regions to be explored include translucent molecular cloud envelopes, cool neutral clouds, warm neutral clouds, the ionized ISM of the Galactic disk and halo, supernova remnants, and hot gas associated with bubbles/supershells in the Magellanic Clouds. The FUSE Team will also observe sight lines to quasars and active galactic nuclei to study high velocity clouds, the distant Galactic halo and intergalactic gas in the low redshift universe. A portion of the observing time will be used for short snapshot exposures to determine the best sight lines for extended observations. The primary objectives of the D/H and O VI programs are listed below in §2.1 and §2.2.

2.1. Goals of the FUSE Team D/H Program

Most of the deuterium in the Universe was created within a few minutes of the Big Bang, and it is generally believed that the net abundance of deuterium decreases with time due to stellar processing (astration). The present day value of the deuterium abundance should therefore reflect the imprint of Big Bang nucleosynthesis as well as the subsequent chemical evolution of the Universe. To understand this history, it is necessary to disentangle local effects from global effects on the D/H ratio, and to integrate the results for a large number of regions into a coherent description of the zero-redshift abundance of deuterium. To this end, the FUSE Team has outlined the following objectives:

- 1) Quantify the effects of local environmental conditions and processes (e.g., astration, fractionation, ionization, metal production) on the measured abundance of deuterium.
- 2) Determine whether the D/H ratio varies within the Milky Way and the implications variability would have for the chemical evolution and mixing of the interstellar medium.
- 3) Determine the D/H ratio in environments with a range of metallicities to use as zero redshift benchmarks for D/H values obtained for low metallicity systems at high redshift.
- 4) Integrate the Milky Way D/H results with chemical evolution models to provide a clearer understanding of galactic chemical evolution, the baryonic content of the Universe, and Big Bang nucleosynthesis.

2.2. Goals of the FUSE Team O VI Program

O VI is the primary far-UV line diagnostic of hot ($T \sim 3 \times 10^5$ K), collisionally ionized gas in the interstellar medium. The production, distribution, and quantity of interstellar gas in this temperature regime outside the local region of the ISM surveyed by *Copernicus* is unknown. Since the processes that create hot gas (e.g., supernovae) are closely related to the physical properties of the ISM, star-formation, heavy element production, the transport of mass and energy, and the chemical evolution of galaxies, the FUSE Team has defined the following objectives:

- 1) Study the physical processes that create interstellar O VI and quantify the role of the hot ISM in controlling the physical properties, distribution, and chemical evolution of gas in the Galaxy.
- 2) Study the transport of energy and matter in the Galaxy and the effects of a “disk-halo connection” on the maintenance of a hot Galactic corona.
- 3) Determine the three dimensional distribution of local hot gas and study the hot/warm gas interfaces at the Local Cloud/Local Bubble boundaries.
- 4) Understand how hot interstellar gases in the Milky Way, LMC, and SMC are related to large scale ISM structures (supernova remnants, supershells, radio loops, etc.), and apply this knowledge to studies of galaxies and quasar absorption line systems.

2.3. Focused Investigations and the FUSE Archive

In addition to the D/H and O VI programs, the FUSE Science Team will conduct studies in a number of areas using data from the key programs as well as supplemental observations. These investigations will include studies of H₂ and the CO/H₂ ratio, hot star winds and atmospheres, cool star chromospheres, supernova remnants (including SN 1987A), cooling flows, active galactic nuclei, jets and circumstellar disks, and planetary atmospheres. A high-resolution measurement of the He II Gunn-Peterson effect will also be made if in-orbit background levels are sufficiently low.

For the first cycle of operations, 63 Guest Investigator programs have been selected to address many intriguing astronomical questions. The data from Team and GI investigations will provide a wealth of information long after the mission has ended. FUSE data will have a six month proprietary period and will be archived at the Space Telescope Science Institute in Baltimore, Maryland.

3. FUSE and High Velocity Clouds

The properties of high velocity clouds (HVCs) are poorly known despite several decades of study. This is due in large part to the general lack of spectroscopic information at ultraviolet wavelengths. Key pieces of information, such as the metallicity and ionization of the HVCs, have remained elusive. This situation has improved in recent years as absorption line observations toward quasars and active galactic nuclei have been conducted with the *Hubble Space Telescope* (HST). For example, Lu *et al.* (1998) have found that HVC 287+22+240 has a metallicity $(S/H) \sim 0.25(S/H)_{\odot}$, with a dust to gas ratio traced by (S/Fe) similar to that in the Magellanic Clouds. This determination rests critically upon the assumption that the ionization correction for the amounts of S II and Fe II arising in ionized gas associated with the HVCs are small [i.e., $N(S)/N(Fe)/N(H) \approx N(S\ II)/N(Fe\ II)/N(H\ I)$]. Using HST data, Wakker and collaborators (this volume) have found $(S/H) \sim 0.1(S/H)_{\odot}$ for Complex C in the direction of Mrk 290. This determination appears fairly robust, as additional information about ionized gas is available from H α imaging of the sight line. The most complete set of HST measurements for studying ionization in high velocity clouds exists for the “C IV-HVCs” toward Mrk 509 (Sembach *et al.* 1999, this volume).

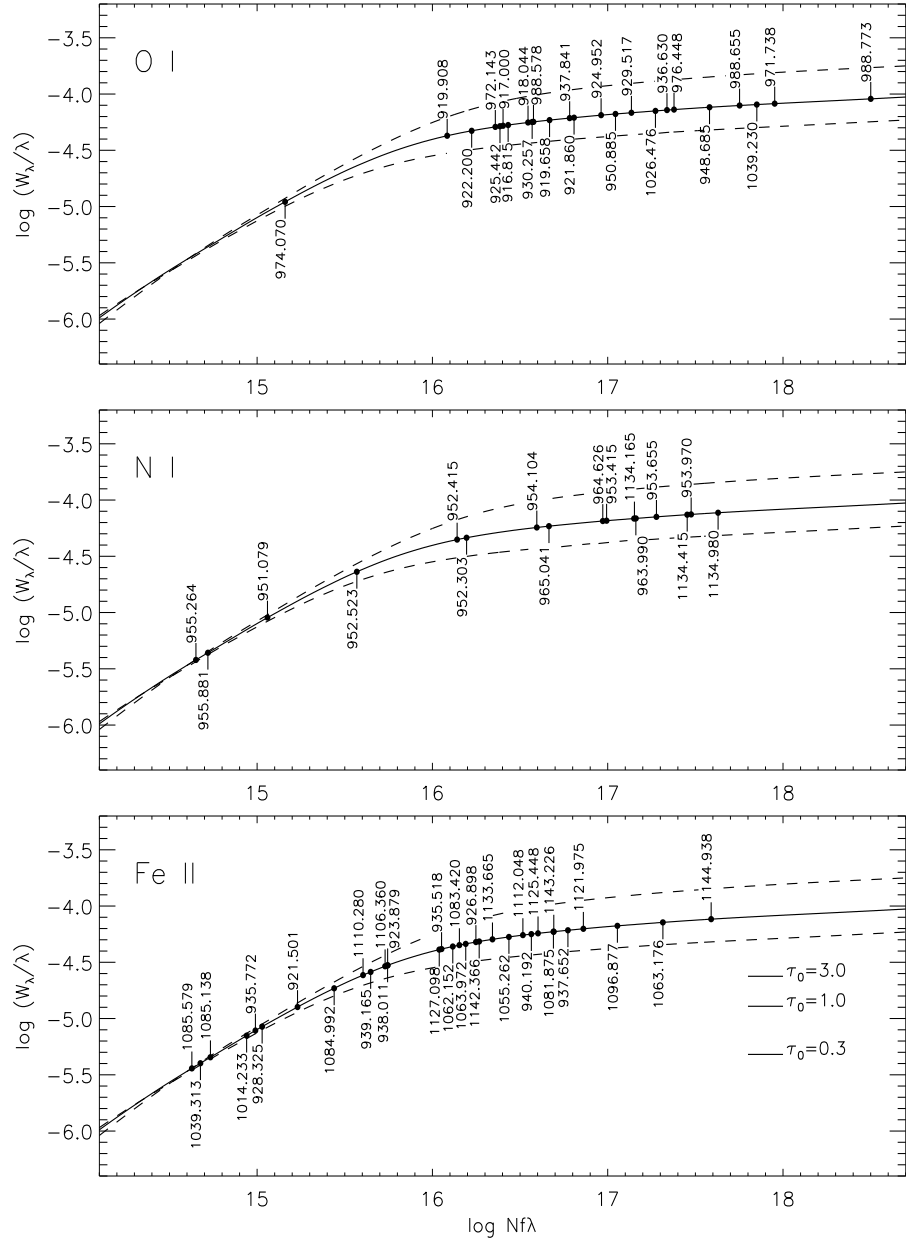


Figure 2. - Curve of growth for O I (top), N I (middle), and Fe II (bottom) lines in the FUSE bandpass. The data points are appropriate for a single component model with a Doppler width of 5 km s^{-1} , $N(\text{H I}) = 1 \times 10^{20} \text{ atoms cm}^{-2}$, and solar abundances. Weak lines that are badly blended with other lines are not shown. The dashed lines are curves for Doppler widths of 3 km s^{-1} (lower curve) and 10 km s^{-1} (upper curve). The inset horizontal tick marks in the Fe II panel indicate the values of $\log(W_\lambda/\lambda)$ for $\tau_0 = 0.3, 1.0, \text{ and } 3.0$.

3.1. Abundances

FUSE observations will provide valuable information for determining the metallicities and ionization of HVCs. In particular, measurements of O I, which has

an ionization potential of 13.6 eV and is strongly tied to H I through charge exchange reactions (Spitzer 1978), will yield oxygen abundances for neutral clouds. Reliable oxygen abundances currently exist for very few clouds, since the two primary transitions in the HST wavelength region are either heavily saturated in most directions ($\lambda 1302.168$) or extremely weak ($\lambda 1355.598$) (see Meyer, Jura, & Cardelli 1998).

Besides containing O I lines, the FUSE bandpass encompasses lines of abundant elements that will be useful for estimating gas-phase abundances in the neutral ISM and HVCs. Several atomic species have lines spanning a large range in $f\lambda$ (e.g., O I, N I, and Fe II). Curves of growth for these species are shown in Figure 2 for $N(\text{H I}) = 1 \times 10^{20}$ atoms cm^{-2} and no gas-phase depletion onto dust. For other values of $N(\text{H I})$ and depletions, D , the lines move horizontally along these curves by an amount equal to $\log N(\text{H I}) + D - 20$. Additional low ionization lines of C II, Mg II, Al II, Si II, P II, and Ar I are plotted on the curve of growth shown in Figure 3. The strong line of C II $\lambda 1036$ and the stronger O I and N I lines shown in Figure 2 are likely to be heavily saturated in their cores along many sight lines but can be used to trace low density, high velocity dispersion gas in their absorption wings. Weak Mg II lines near 1026\AA will be difficult to recover in the wings of H I Ly β and are not shown in Figure 3. For information about local ISM abundances derived from *Copernicus* data, see Jenkins, Savage, & Spitzer (1986) and Jenkins (1987, and references therein).

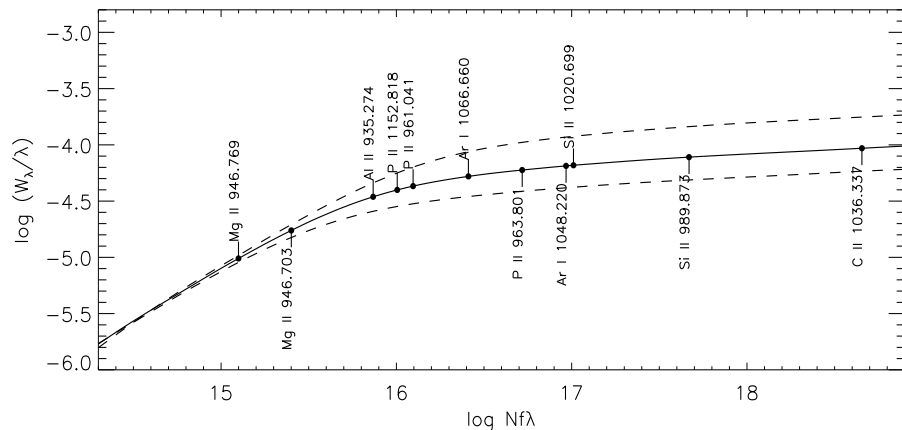


Figure 3. Curves of growth for far-UV lines of various heavy element species not shown in Figure 2. Values for Cl I and Cl II are not shown. The data points are appropriate for a single component model with a Doppler width of 5 km s^{-1} , $N(\text{H I}) = 1 \times 10^{20}$ atoms cm^{-2} , and solar abundances. The dashed lines are curves for Doppler widths of 3 km s^{-1} (lower curve) and 10 km s^{-1} (upper curve).

The primary obstacle facing abundance studies of HVCs is the difficulty in making accurate determinations of neutral hydrogen column densities through 21 cm emission since some HVCs appear to contain structure at arc minute scales (c.f., Wakker & van Woerden 1997). FUSE observations of higher order Lyman series lines of H I will probably not address this problem, except in special circumstances. It might be possible to do so when the velocity of the HVC is large ($|V_{\text{LSR}}| \sim 200 \text{ km s}^{-1}$), the width of the low velocity absorption is small ($\text{FWHM} < 50 \text{ km s}^{-1}$), and the amount of intermediate velocity gas is negligible

($N(\text{H I}) < \text{few} \times 10^{16}$ atoms cm^{-2}). Detections in multiple H I lines will be necessary since a typical HVC H I column density of $\sim 10^{19}$ atoms cm^{-2} will place most of the H I lines on the flat part of the curve of growth.

3.2. Ionization

Absorption line observations of ionized gas species in some HVCs indicate that they can contain large quantities of ionized gas (Sembach *et al.* 1995, 1999, this volume). $\text{H}\alpha$ imaging of the larger HVC complexes (Tufté, Reynolds, & Haffner 1998, this volume) also reveals the presence of ionized gas. Therefore, it is important to consider whether gas-phase abundances derived from measurements of singly charged ions (e.g., S III, P II, Fe II) or neutral atoms with first ionization potentials greater than 13.6 eV (e.g., N I, Ar I) are affected by H II region contributions. Lines of adjacent ionization stages of many elements in the far-UV (e.g., C I-III, N I-III, P II-V, S III-IV, Cl I-II, Ar I-II, and Fe II-III) can be used to estimate ionization corrections when necessary.

Ionized gas diagnostics in the far-UV wavelength region span a large range in ionization potential. Of these, the strong O VI lines are the most important for studying gases with $T \geq 10^5$ K. The observable lines of other elements trace lower temperature gases ranging from 10^4 to $\sim 10^5$ K. Table 1 contains a list of the ionized gas resonance lines in the FUSE bandpass. Lines of species having creation ionization potentials greater than 13.6 eV are included. For each ion, predicted line strengths and widths are listed for a simple model in which a solar metallicity gas with no dust and $N(\text{H II}) = 1 \times 10^{20}$ cm^{-2} is in collisional ionization equilibrium. In non-equilibrium situations, the ionization fractions will differ from those listed (see Sutherland & Dopita 1993).

Some of the lines listed in Table 1 are very strong and will be heavily saturated even when $N(\text{H II})$ is low. For example, $\tau_0(\text{C III } \lambda 977) > 3$ when $N(\text{H II}) > \text{few} \times 10^{16}$ atoms cm^{-2} . Lines of other ions, such as P III, P V, and Cr III, will be weak even when $N(\text{H II})$ is large. Incorporation of the refractory elements (e.g., Cr, Fe) into dust will affect the observed line strengths of Cr III and Fe III.

3.3. Molecules

FUSE will be able to search for dust and molecules in HVCs. Comparisons of Fe to O and other lightly depleted elements will reveal whether the gas has a solar abundance pattern, independent of whether the H I column density is known. Searches for H_2 absorption will reveal columns as small as 10^{14} molecules cm^{-2} , or about 5 orders of magnitude lower than has been possible with millimeter wavelength observations of CO (e.g., Wakker *et al.* 1997).

3.4. FUSE Team Observations of HVCs

Observations of high velocity clouds (HVCs) play prominent roles in the FUSE D/H and O VI programs. Table 2 contains a list of selected HVCs toward objects that will be observed in detail by the FUSE Science Team. The Galactic coordinates of the background sources, HVC identifications, and velocities of the HVCs are listed. The extragalactic sight lines listed currently have planned observations sufficient to produce $S/N \geq 10$ per FUSE resolution element. An additional ~ 50 – 100 extragalactic sight lines will be inspected at low resolution to determine far-UV flux levels and sight line velocity structure. Many of these

Table 1. Ionized Gas Resonance Lines in the FUSE Bandpass^a

Ion	Z	A	IP ^(i,i+1) (eV)	T _{max} (K)	f _{ion}	λ (Å)	log fλ	τ ₀	b ₀ (km s ⁻¹)
C III	6	8.55	24.38, 47.89	70,000	0.832	977.020	2.872	3340	9.8
N II	7	7.97	14.53, 29.60	25,000	0.971	915.612 1083.990	2.123 2.048	330 278	5.4 5.4
N III	7	7.97	29.60, 47.45	80,000	0.769	989.799	2.023	116	9.7
O VI	8	8.87	113.9, 138.1	280,000	0.220	1031.926 1037.617	2.137 1.836	196 98	17.1 17.1
P III	15	5.57	19.72, 30.18	35,000	0.792	998.000	2.047	1.1	4.3
P IV	15	5.57	30.18, 51.37	70,000	0.706	950.657	3.044	7.1	6.1
P V	15	5.57	51.37, 65.02	100,000	0.609	1117.977 1128.008	2.723 2.422	2.4 1.2	7.3 7.3
S III	16	7.27	23.33, 34.83	50,000	0.838	1012.502	1.556	16.5	5.1
S IV	16	7.27	34.83, 47.30	100,000	0.610	1062.662	1.628	10.0	7.2
S VI	16	7.27	72.68, 88.05	180,000	0.140	933.378 944.523	2.319 2.615	16.6 8.3	9.7 9.7
Ar II	18	6.56	15.76, 27.63	22,000	0.964	919.781	0.912	1.4	3.0
Cr III	24	5.68	16.50, 30.96	28,000	0.893	923.780 1030.100 1033.331 1040.050	1.874 1.809 1.820 2.104	1.6 1.4 1.4 2.7	3.0 3.0 3.0 3.0
Fe III	26	7.51	16.18, 30.65	28,000	0.893	1122.526	1.947	132	2.9

^aThis table contains information for ionized gas lines in the 905–1187Å wavelength region. Fine structure transitions of N II and N III occur at wavelengths within 1–2Å of the N II and N III lines listed in this table. Columns 2–9 are as follows:

Z: Atomic number.

A: Solar abundance of element (total of all ions) relative to H on a logarithmic scale where A(H) = 12.00.

IP: Ionization potential to create and destroy the listed ion (Moore 1971).

T_{max}: Temperature at which ion peaks in abundance in collisional ionization equilibrium. Values are from Sutherland & Dopita (1993), except for P and Cr. The values for P were obtained by interpolating along iso-electronic sequences of adjoining even-Z elements (Si, S). For Cr III, a value equal to those for Fe III and Ni III was adopted.

f_{ion}: Fractional abundance of ion in collisional ionization at temperature T_{max}.

λ: Wavelength from Morton (1991).

log fλ: Product of wavelength (in Å) and f-value from Morton (1991).

τ₀: Optical depth of line at line center for a plasma with N(H II) = 1x10²⁰ cm⁻², assuming collisional ionization equilibrium, the listed values of A, T_{max}, f_{ion}, and b₀, solar metallicity, and no gas-phase depletion due to dust.

b₀: Thermal broadening parameter of line at temperature T_{max}.

“snapshot” sight lines pass through or near Complexes A, C, and M. The three Galactic sight lines listed have HVCs that have been observed in absorption and represent a small subset of the total number of Galactic sight lines that will be observed.

Table 2. **Selected High Velocity Cloud Sight Lines in the FUSE Science Team Program^a**

Object	HVC Name	$l(^{\circ})$	$b(^{\circ})$	$V_{\text{LSR}}(\text{km s}^{-1})$
Extragalactic Sight Lines ^a				
PKS 2155-304	C IV-HVCs	17.7	-52.2	-140, -256
Mrk 509	C IV-HVCs	36.0	-29.9	-228, -283
Mrk 290	Complex C	91.5	+48.0	-136
H 1821+643	Outer Arm	94.0	+27.4	-120
Mrk 817	Complex C	100.3	+53.5	-107
NGC 3783	HVC 287+22+240	287.5	+23.0	+240
Fairall 9	Magellanic Stream	295.1	-57.8	+170, +210
Galactic Sight Lines ^b				
LS 4825	Inner Galaxy	1.7	-6.6	-206, -150, +93
BD +38 2182	Complex M	182.2	+62.2	-93
HD 156359	Uncatalogued	328.7	-14.5	+125

^aObservations of stars in the Large and Small Magellanic Clouds will also provide information on high velocity gas in those directions. Additional HVCs along extragalactic sight lines may be explored through the D/H snapshot program, which will produce short exposures of 50–100 extragalactic objects.

^bThese are but a few of the many Galactic sight lines that will be observed by FUSE. This table does not include the numerous intermediate velocity clouds or high velocity gas features associated with known supernova remnants (e.g., Vela) or star-forming regions (e.g., Carina) that will be observed. Approximately 200 sight lines in the Galactic disk and halo will be observed as part of the D/H and O VI programs

4. Simulated Spectra for Simple H I Cloud Models

Given the large number of atomic and molecular transitions in the far-UV suitable for studies of HVCs, it is instructive to consider the absorption signatures expected for simple interstellar cloud properties. These results can then be applied to more complicated situations.

4.1. Absorption Lines Viewed at FUSE Resolution

The *apparent* optical depth of a spectral line at a velocity v is given by $\tau_a(v) = \ln(I_c(v)/I_o(v))$, where I_o and I_c are the observed and continuum (unattenuated) intensities, respectively. This differs from the true optical depth, $\tau(v) = \ln(I_c(v)/I(v))$, due to the finite resolution of the spectral spread function of the instrument used to observe the absorption line. The effect of this convolution on the line shape of a single Gaussian component is shown in Figure 4 for three values of the Doppler width b_0 and central optical depth τ_0 of the line. An instrumental spread function width appropriate for FUSE, $b_I = (c\lambda/\Delta\lambda)/(2\sqrt{\ln 2}) \approx 6 \text{ km s}^{-1}$, has been applied. The more severely a line is under-resolved by the instrument, the greater the difference between the true optical depth of the line and its apparent optical depth. The resulting unresolved saturated structure must be accounted for in determinations of the column density contained within the line. Detailed discussions of apparent optical depths and the derivation of

column densities from apparent optical depth profiles have been given by Savage & Sembach (1991) and Jenkins (1996).

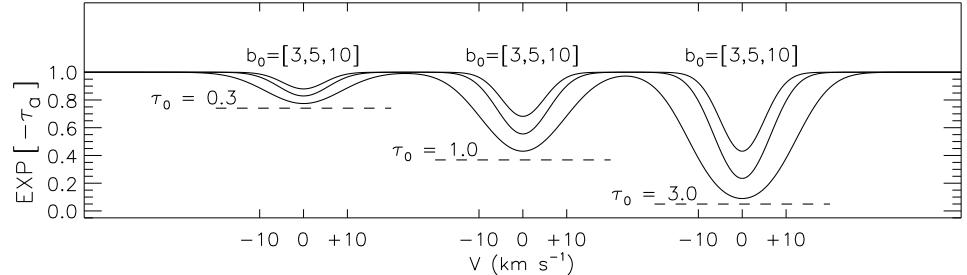


Figure 4. Line profiles of intrinsic widths b_0 and central optical depths τ_0 (left: $\tau_0 = 0.3$, middle: $\tau_0 = 1.0$, right: $\tau_0 = 3.0$) convolved with a Gaussian line spread function having an instrumental resolution appropriate for FUSE, $(\lambda/\Delta\lambda) \approx 30,000$.

4.2. Model 1: A Sight Line Through the Neutral Medium of the Galactic Halo

Figure 5 contains a noiseless simulation of the absorption expected in the 910–1160 Å spectral region for a single interstellar cloud containing 3×10^{20} atoms cm^{-2} of H I and 1×10^{17} molecules cm^{-2} of H₂. The cloud has a temperature of 100 K, a b-value (thermal + turbulent) of 5 km s^{-1} , and a warm halo cloud gas-phase depletion pattern (Savage & Sembach 1996).¹ The model includes lines having $\tau_0 > 0.05$ and an instrumental resolution appropriate for FUSE. Lines of atomic species and H₂ are indicated at the top of each panel. The D/H ratio used is the local ISM value of 1.6×10^{-5} (Linsky *et al.* 1993). For elements with first ionization potentials below 13.6 eV, it is assumed that 0.5% of the elemental gas-phase abundance is neutral, with the remaining 99.5% being singly ionized.² Chlorine is an exception since reactions with H₂ can convert Cl II to Cl I (Jura 1974; Jura & York 1978); it is assumed that 20% of the Cl is Cl I and 80% is Cl II, which is typical of low density regions with large values of $N(\text{H I})/N(\text{H}_2)$ (see Harris & Bromage 1984). Table 3 contains a summary of the model parameters.

The richness of the far-UV wavelength region shown in Figure 5 and the progression to higher line densities as wavelength decreases to the Lyman limit at 912 Å is striking. Even for the simple, single component model shown, line blending can be problematic, especially at shorter wavelengths.

Atomic fine-structure lines and molecular lines of HD and CO are not included in this model. Information about additional atomic lines and CO can be found in the data compilations presented by Morton (1991) and Morton & Noreau (1994). Table 4 contains a brief list of some of the transitions in the

¹ Gas-phase depletions for Mg, Al, Si, S, Cr, Mn, Fe, and Ni are included. $[\text{Mg}/\text{H}] = -0.50$, $[\text{Al}/\text{H}] \equiv [\text{Fe}/\text{H}] = -0.60$, $[\text{Si}/\text{H}] = -0.50$, $[\text{S}/\text{H}] = 0.0$, $[\text{Cr}/\text{H}] = -0.50$, $[\text{Mn}/\text{H}] = -0.60$, $[\text{Ni}/\text{H}] = -0.85$. All other elements (X) are assumed to have solar abundances, $[\text{X}/\text{H}] = \log(\text{X}/\text{H}) - \log(\text{X}/\text{H})_{\odot} = 0.0$.

²This is an approximate value. The relative amounts of neutral and singly ionized species will depend upon the detailed physical conditions of the cloud.

Table 3. **Model Parameters for Simulated Spectra^a**

Parameter	Model 1 (Figure 5)	Model 2 (Figure 6)
N(H I) (cm ⁻²)	3 × 10 ²⁰	1 × 10 ²⁰
N(H ₂) (cm ⁻²)	1 × 10 ¹⁷	1 × 10 ¹⁷
<i>b</i> ₀ (km s ⁻¹)	5	5
<i>v</i> ₀ (km s ⁻¹)	0	0
T (K)	100	500
Metallicity	Solar	Solar
Dust	Warm halo	None
D/H ratio	1.6 × 10 ⁻⁵	1.6 × 10 ⁻⁵
<i>b</i> _I (km s ⁻¹)	5.9	5.9
<i>τ</i> _{thresh}	0.05	0.05
No. of lines (atomic, H ₂)	302, 190	278, 393

^aThe models shown in Figures 5 and 6 are appropriate for a single interstellar cloud with the parameters listed in this table. The solar abundances used are meteoritic values from Anders & Grevesse (1989), except for C, N, and O, which are photospheric values from Grevesse & Noels (1993). The Savage & Sembach (1996) warm halo cloud gas-phase depletion pattern due to dust is used in Model 1; elements not included in their study are assumed to have solar abundances, except for Al, which is set to the value for Fe and Ni. The atomic and H₂ data in these models are from Morton (1991) and Abgrall *et al.* (1993a, 1993b).

Lyman ($B^1\Sigma_u^+ - X^1\Sigma_g^+$) and Werner ($C^1\Pi_u - X^1\Sigma_g^+$) systems of HD. The wavelengths are from Dabrowski & Herzberg (1976). The *f*-values for these lines were computed using the band oscillator strengths calculated by Allison & Dalgarno (1970). Some of these transitions were seen in the spectrum of ζ Ophiuchi by *Copernicus* (Wright & Morton 1979).

4.3. Model 2: An H I Cloud with Warm H₂

Figure 6 contains a second sample spectrum of the same cloud in Figure 5 with a lower value of N(H I), a temperature of 500 K, and no gas-phase depletion onto dust grains. Other model parameters are summarized in Table 3. In this case, higher order ($J \geq 3$) rotational lines of H₂ blanket the spectrum.

The models shown in Figures 5 and 6 are intended to serve as aids in identifying lines of various elemental species in the FUSE wavelength range. These figures can be used to estimate line strengths for different cloud parameters through the following scaling relation:

$$\tau_0 \propto \frac{N(\text{H I})}{b_0} 10^{(A+D)},$$

where τ_0 is the optical depth at line center, N(H I) is the column density of H I, b_0 is the Doppler spread parameter for the line, A is the logarithmic abundance of the element on a scale where A(H) = 12.00, and D is the logarithmic gas-phase depletion of the element relative to the reference abundances used. Note that τ_0 is the true optical depth of the line, not the *apparent* optical depth, τ_a , which is less than τ_0 in situations where the instrumental line function width, b_I , is greater than the intrinsic width of the line, b_0 . For most neutral gas species

observed by FUSE, $b_I > b_0$, and therefore $\tau_a < \tau_0$. Figure 4 can be used to relate τ_a and τ_0 for FUSE data.

Table 4. Selected HD Lines in the FUSE Bandpass^a

Transition	$\lambda(\text{\AA})$	f-value	Transition	$\lambda(\text{\AA})$	f-value
$B^1\Sigma_u^+ - X^1\Sigma_g^+$ (Lyman series)					
0-0 R(0)	1105.838*	7.60 (-4)	1-0 R(0)	1091.999*	2.99 (-3)
0-0 R(1)	1106.214*	5.07 (-4)	1-0 R(1)	1092.397*	1.98 (-3)
0-0 P(1)	1107.289*	2.53 (-4)	1-0 P(1)	1093.400*	9.95 (-4)
0-0 R(2)	1107.325*	4.56 (-4)	1-0 R(2)	1093.526*	1.79 (-3)
0-0 P(2)	1109.114*	3.03 (-4)	1-0 P(2)	1095.194*	1.19 (-3)
2-0 R(0)	1078.828*	6.74 (-3)	3-0 R(0)	1066.271	1.14 (-2)
2-0 R(1)	1079.242*	4.49 (-3)	3-0 R(1)	1066.708	7.59 (-3)
2-0 P(1)	1080.182*	2.24 (-3)	3-0 P(1)	1067.585*	3.79 (-3)
2-0 R(2)	1080.381*	4.04 (-3)	3-0 R(2)	1067.842	6.82 (-3)
2-0 P(2)	1081.946*	2.69 (-3)	3-0 P(2)	1069.319	4.54 (-3)
4-0 R(0)	1054.288	1.61 (-2)	5-0 R(0)	1042.847	2.01 (-2)
4-0 R(1)	1054.722†	1.07 (-2)	5-0 R(1)	1043.288	1.34 (-2)
4-0 P(1)	1055.563	5.36 (-3)	5-0 P(1)	1044.082	6.68 (-3)
4-0 R(2)	1055.877	9.64 (-3)	5-0 R(2)	1044.442	1.20 (-2)
4-0 P(2)	1057.266	6.42 (-3)	5-0 P(2)	1045.759	8.00 (-3)
6-0 R(0)	1031.912	2.28 (-2)	7-0 R(0)	1021.456	2.42 (-2)
6-0 R(1)	1032.361	1.52 (-2)	7-0 R(1)	1021.916	1.62 (-2)
6-0 P(1)	1033.114	7.60 (-3)	7-0 P(1)	1022.626	8.07 (-3)
6-0 R(2)	1033.514	1.37 (-2)	7-0 R(2)	1023.064	1.45 (-2)
6-0 P(2)	1034.764	9.11 (-3)	7-0 P(2)	1024.249	9.67 (-3)
8-0 R(0)	1011.457†	2.44 (-2)	9-0 R(0)	1001.892	2.35 (-2)
8-0 R(1)	1011.924	1.63 (-2)	9-0 R(1)	1002.360	1.57 (-2)
8-0 P(1)	1012.590†	8.12 (-3)	9-0 P(1)	1003.003	7.84 (-3)
8-0 R(2)	1013.074	1.46 (-2)	9-0 R(2)	1003.507	1.41 (-2)
8-0 P(2)	1014.195	9.73 (-3)	9-0 P(2)	1004.580	9.39 (-3)
$C^1\Pi_u - X^1\Sigma_g^+$ (Werner series)					
0-0 R(1)	1007.251†	1.73 (-2)	1-0 R(1)	987.276†	3.07 (-2)
0-0 R(0)	1007.283†	3.45 (-2)	1-0 R(0)	987.276†	6.14 (-2)
0-0 R(2)	1007.650	1.38 (-2)	1-0 R(2)	987.712	2.45 (-2)
0-0 Q(1)	1008.199†	1.73 (-2)	1-0 Q(1)	988.145	3.07 (-2)
0-0 Q(2)	1009.080	1.73 (-2)	1-0 Q(2)	989.021	3.06 (-2)
0-0 P(2)	1010.005†	3.45 (-3)	1-0 P(2)	989.893	6.12 (-3)
2-0 R(0)	968.972	6.63 (-2)	3-0 R(0)	952.208	5.72 (-2)
2-0 R(1)	969.030	3.31 (-2)	3-0 R(1)	952.285	2.86 (-2)
2-0 R(2)	969.550	2.65 (-2)	3-0 R(2)	952.802	2.29 (-2)
2-0 Q(1)	969.822	3.31 (-2)	3-0 Q(1)	953.046	2.86 (-2)
2-0 Q(2)	970.697	3.31 (-2)	3-0 Q(2)	953.945†	2.85 (-2)
2-0 P(2)	971.490	6.61 (-3)	3-0 P(2)	954.637†	5.70 (-3)

^aVacuum wavelengths in this table are from the wavenumbers measured by Dabrowski & Herzberg (1976). A dagger (†) next to the wavelength indicates that the line may be blended in their spectrum. An asterisk (*) indicates that the wavelengths are calculated from the rotational constants and band origins listed by Dabrowski & Herzberg (1976). The f-values are based upon the band oscillator strengths calculated by Allison & Dalgarno (1970). A value of 1.23 (-4) is equivalent to 1.23×10^{-4} .

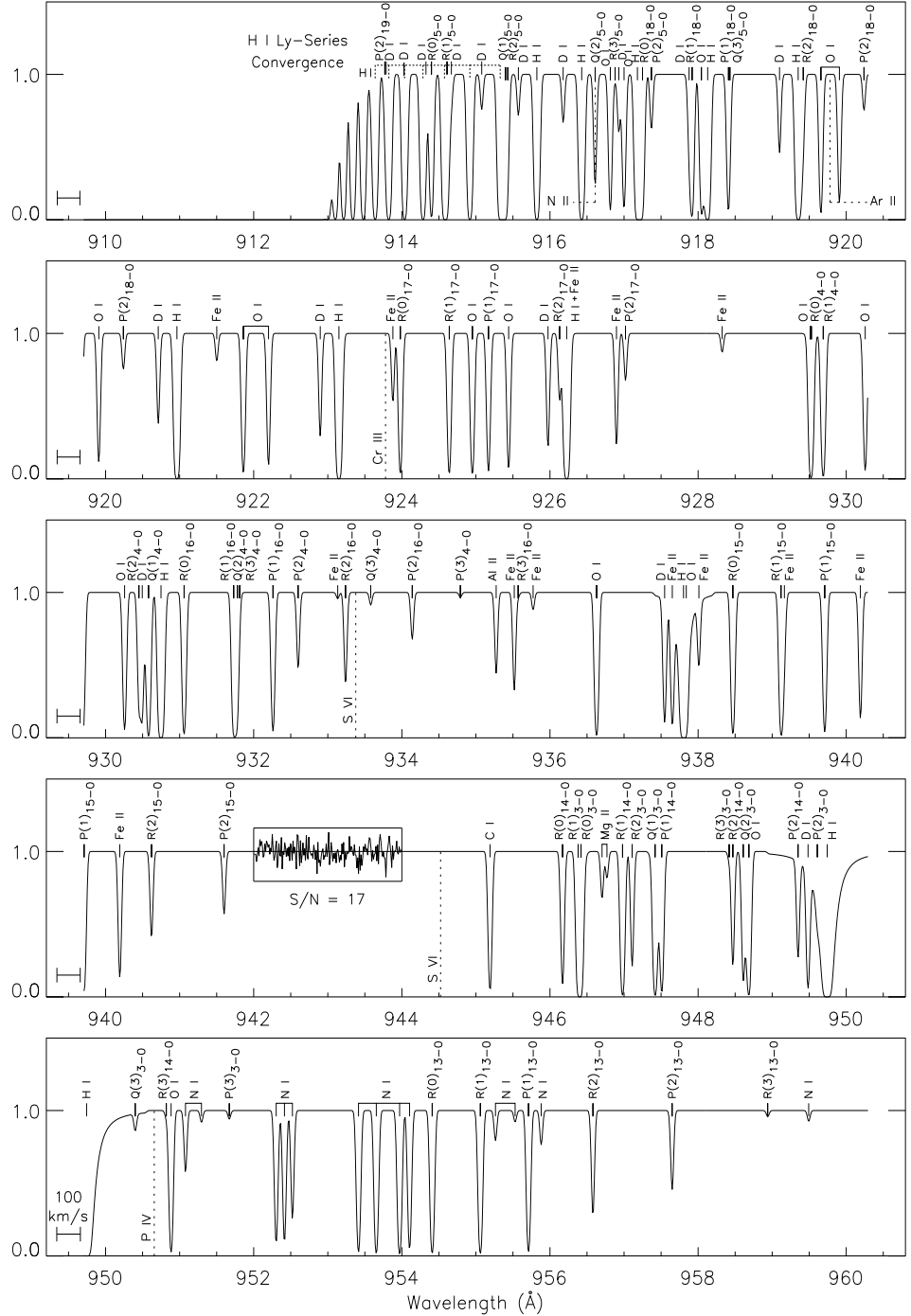


Figure 5a. - Model spectrum #1 (H I halo cloud sight line). The parameters for this model are listed in Table 3. Vertical dashed lines indicate the wavelengths of the ionized gas lines listed in Table 1. Fine structure lines of C I, C II, N II, and N III are not shown. The inset box shows a Poisson noise level $S/N = 17$ per FUSE pixel, which corresponds to $S/N = 30$ per resolution element (3 pixels). The horizontal error bar in the lower left of each panel indicates a velocity range of 100 km s^{-1} .

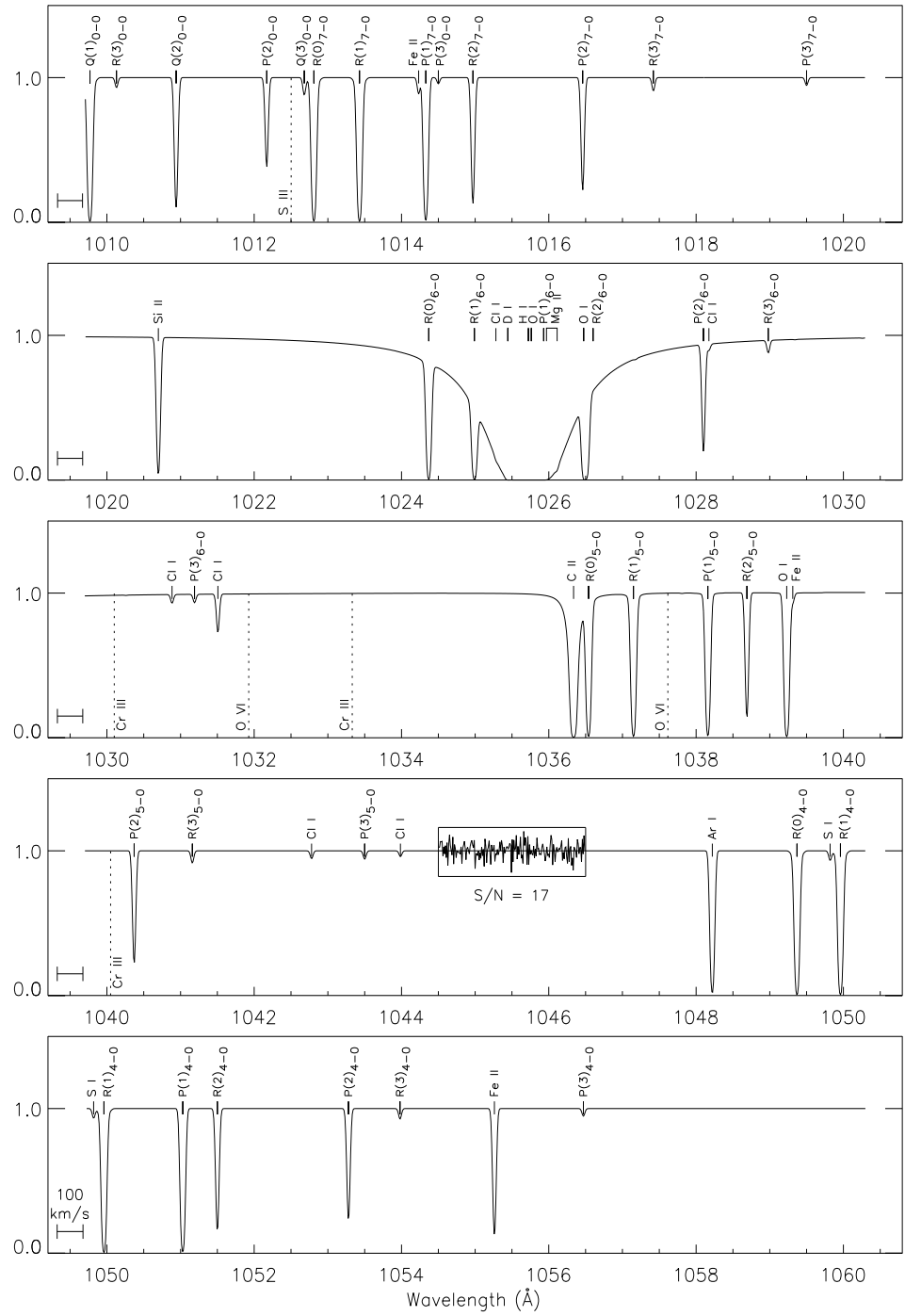


Figure 5c. Same as Figure 5a, except for the 1010–1060 Å wavelength region.

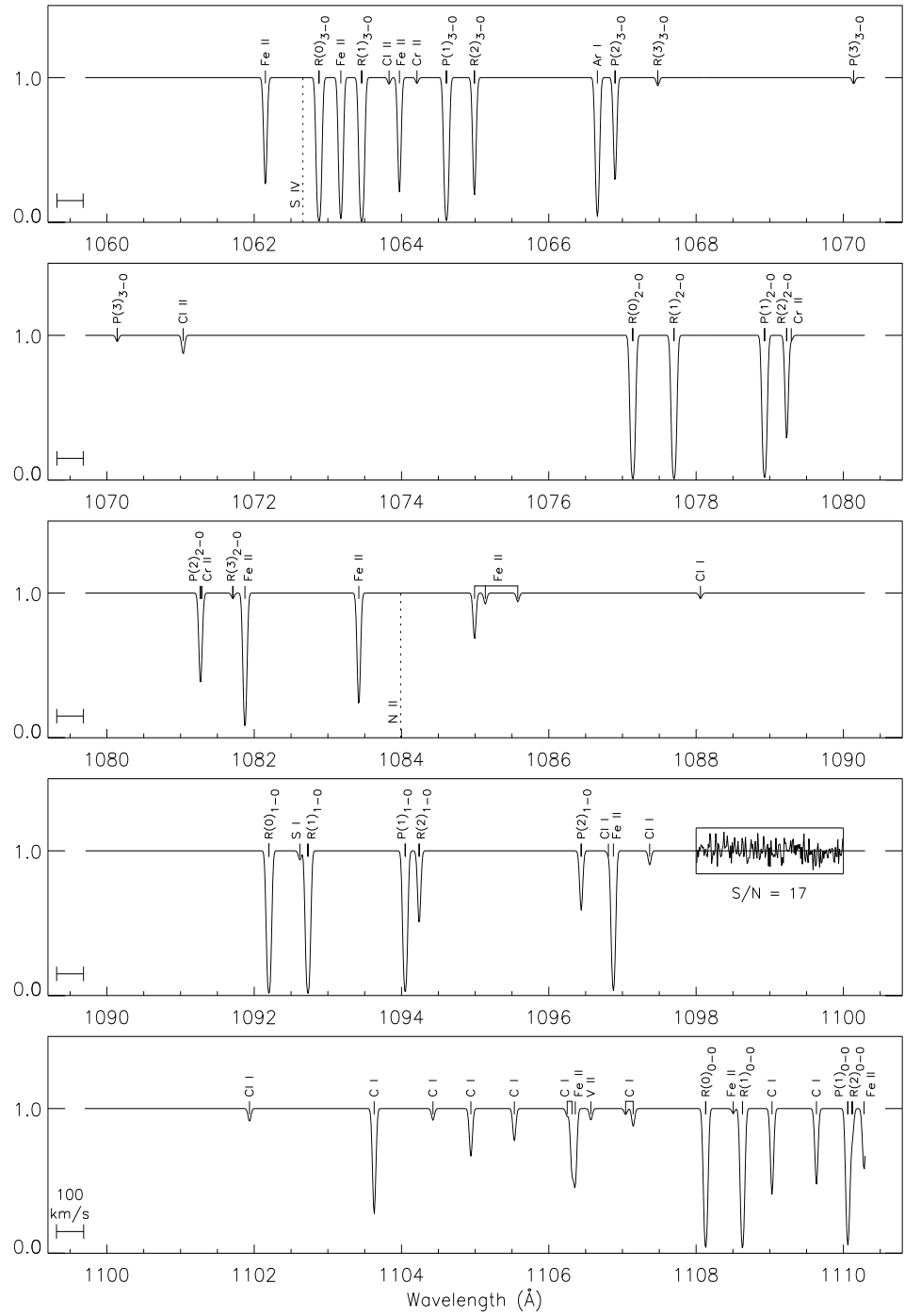


Figure 5d. Same as Figure 5a, except for the 1060–1110 Å wavelength region.

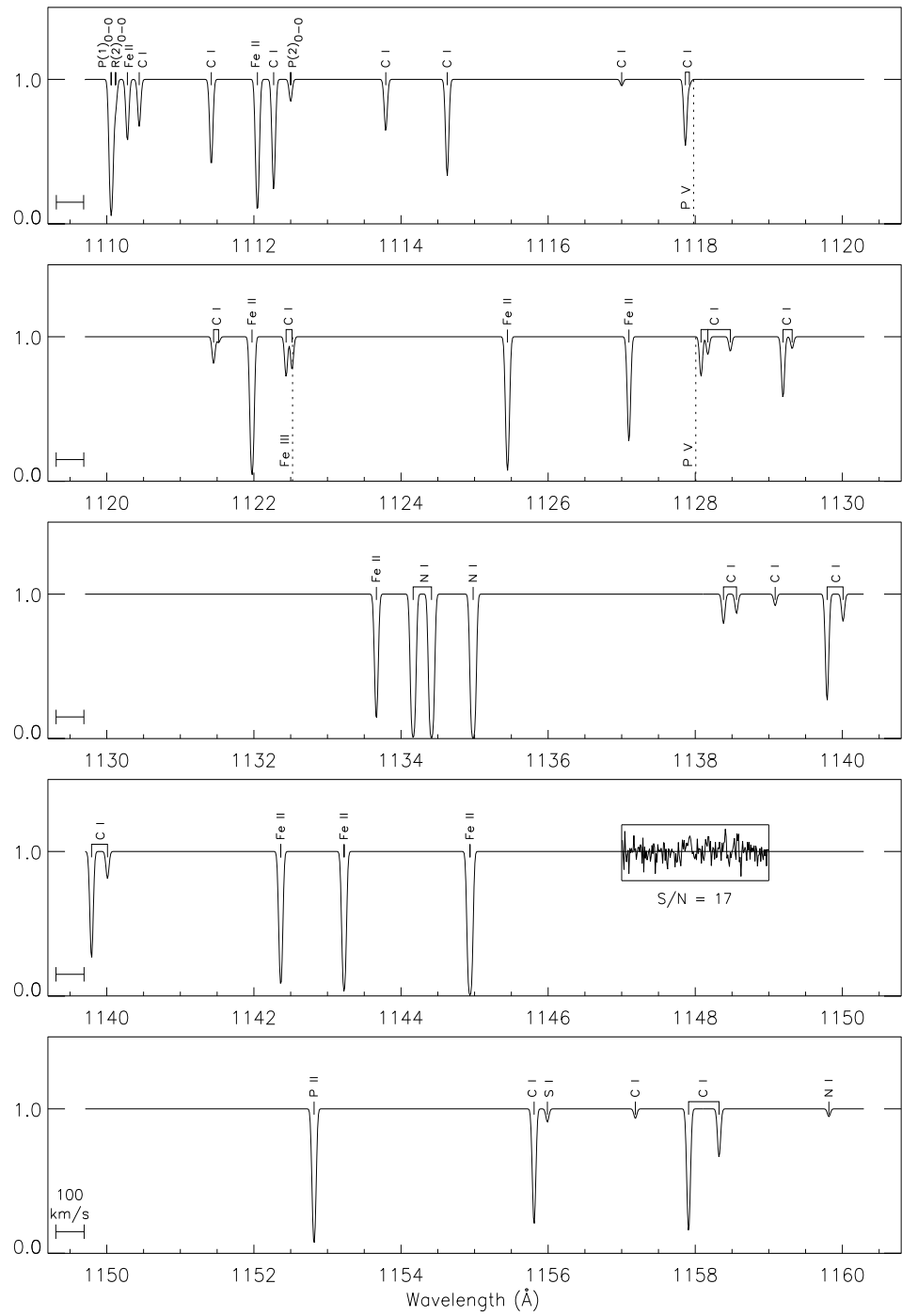


Figure 5e. Same as Figure 5a, except for the 1110–1160 Å wavelength region.

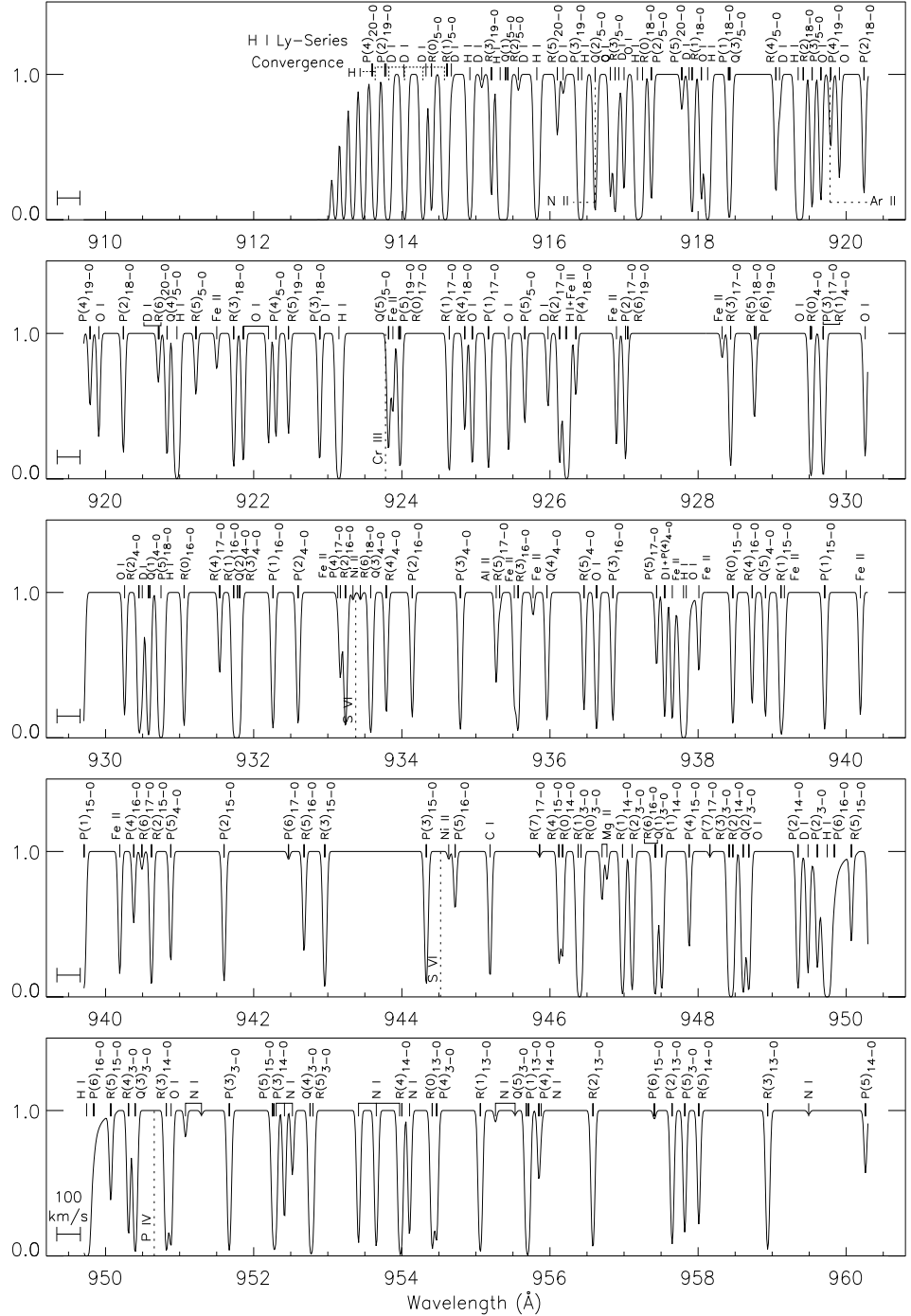


Figure 6a. Model spectrum #2 (H I, warm H₂ sight line). The parameters for this model are listed in Table 3. Vertical dashed lines indicate the wavelengths of the ionized gas lines listed in Table 1. Fine structure lines of C I, C II, N II, and N III are not shown. The horizontal error bar in the lower left of each panel indicates a velocity range of 100 km s⁻¹.

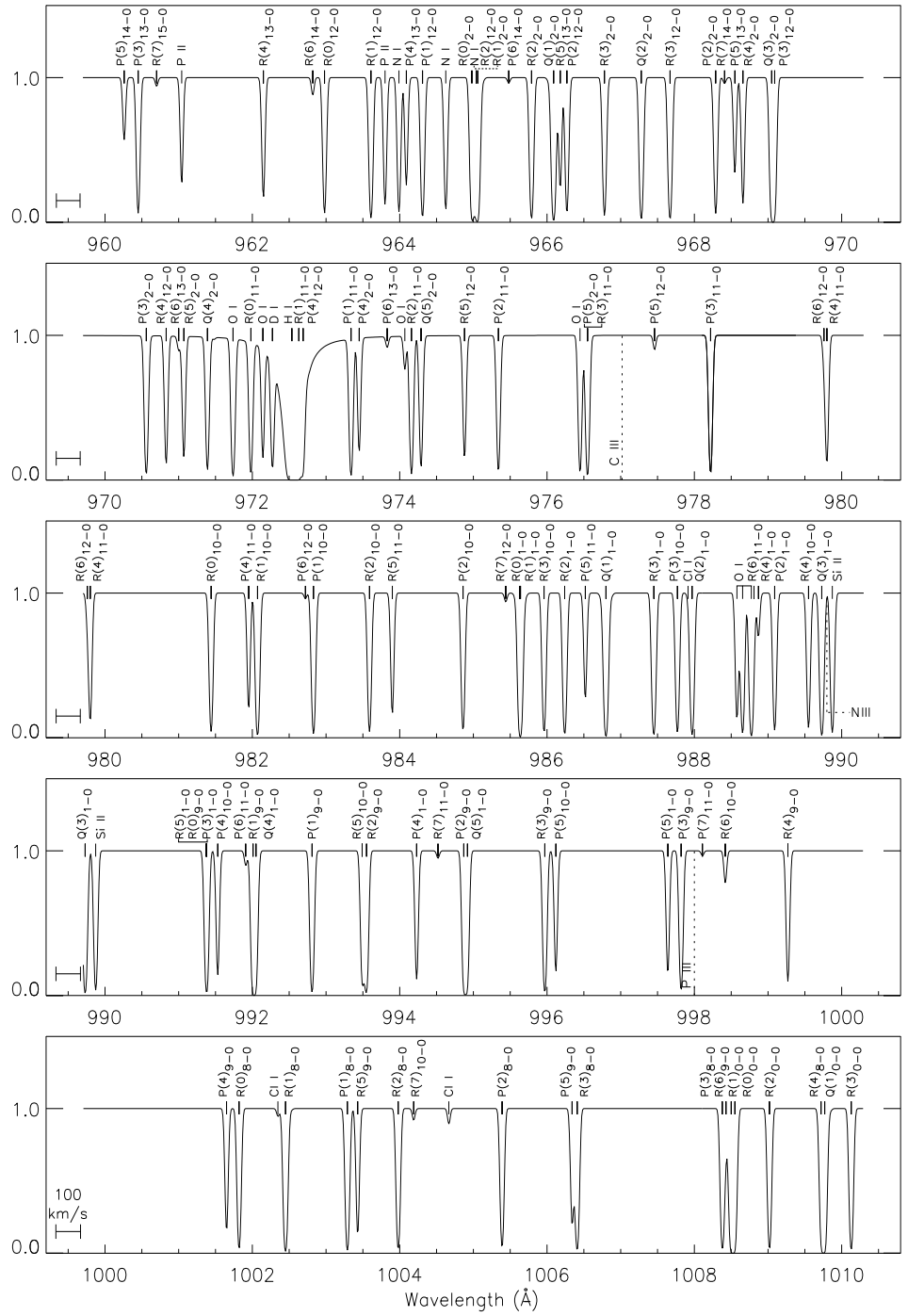


Figure 6b. Same as Figure 6a, except for the 960–1010 Å wavelength region.

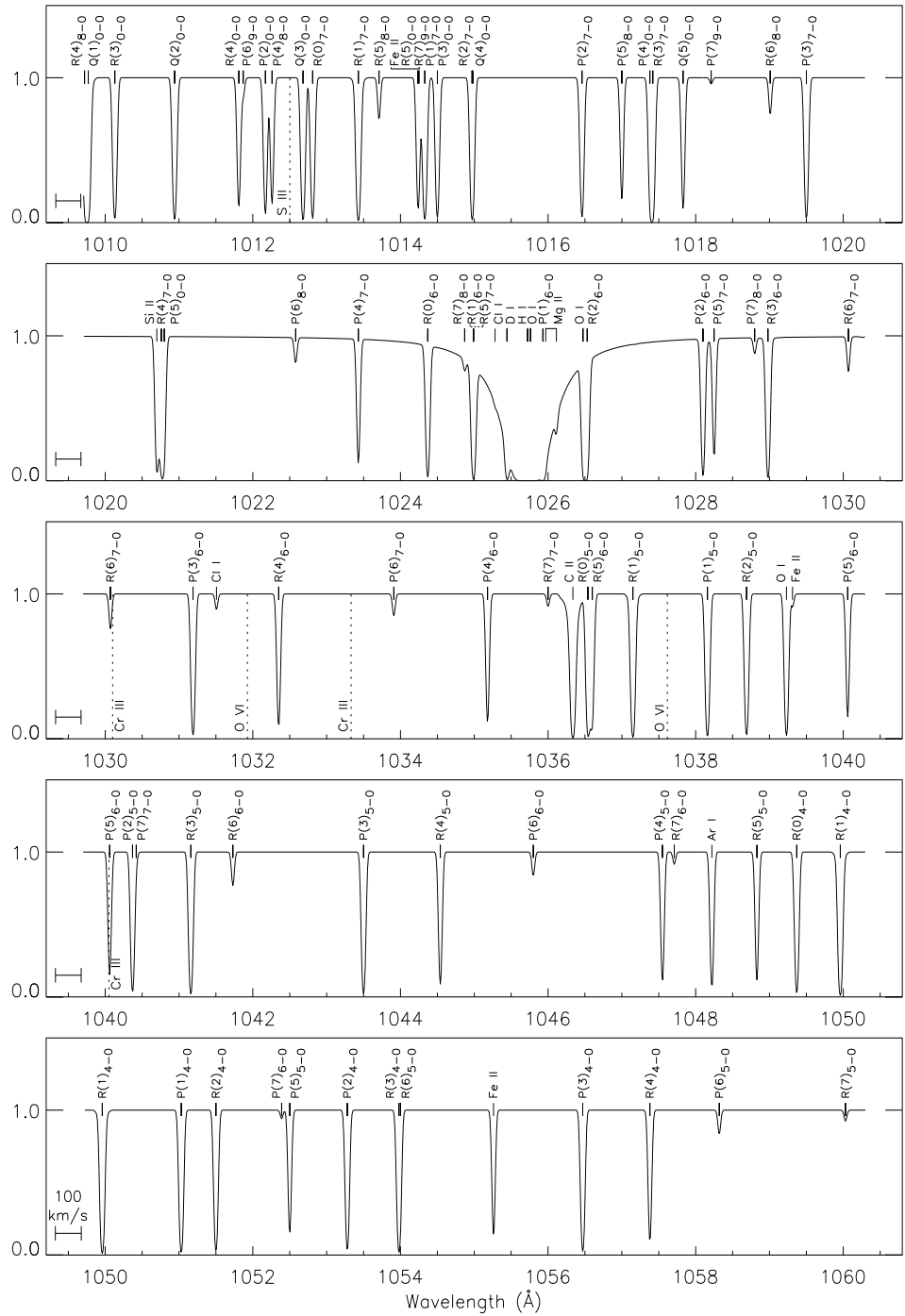


Figure 6c. Same as Figure 6a, except for the 1010–1060 Å wavelength region.

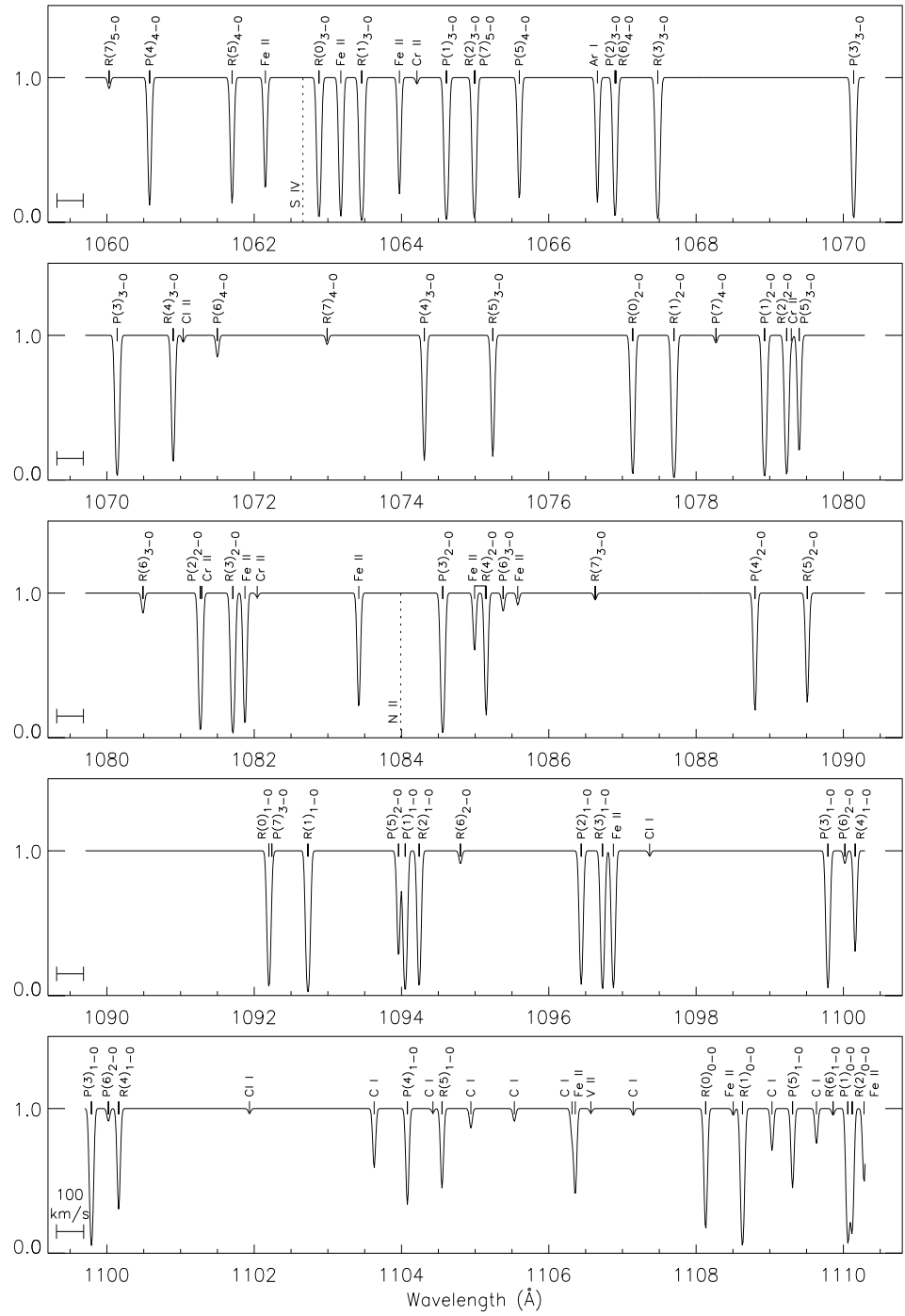


Figure 6d. Same as Figure 6a, except for the 1060–1110 Å wavelength region.

5. Science Team Members

FUSE is a Principal Investigator class mission with a Science Team composed of U.S., Canadian, and French scientists at academic and government institutions. The Principal Investigator of the FUSE mission is H. Warren Moos of the Johns Hopkins University. Members of the FUSE Science Team include: Webster Cash, Lennox Cowie, Arthur Davidsen, Andrea Dupree, Paul Feldman, Scott Friedman, James Green, Richard Green, Cecile Gry (associate), John Hutchings, Edward Jenkins, Jeffrey Linsky, Roger Malina, Blair Savage, J. Michael Shull, Oswald Siegmund, George Sonneborn, Theodore Snow, Alfred Vidal-Madjar, Alan Willis (associate), Bruce Woodgate, and Donald York.

In addition to the Science Team, there are numerous members of the FUSE Instrument and Operations Teams at the Johns Hopkins University, the University of Colorado, and the University of California who have contributed to the instrumental development, mission planning, science planning, and science operations of FUSE. These scientists will actively participate in the analysis of data obtained with Science Team observing time.

6. The FUSE Satellite

The FUSE satellite is composed of a three-axis stabilized spacecraft and the scientific instrument. The total satellite weight is 1360 kg. The instrument consists of four co-aligned telescopes optimized for transmission at far-UV wavelengths. The light from the four channels is dispersed by four spherical, aberration-corrected holographic diffraction gratings. Two channels with SiC coatings cover 905–1100Å, and two channels with Al+LiF coatings cover 1000–1187Å. Two delay-line microchannel plate detectors each detect one SiC and one Al+LiF channel.

Wavelength overlap, physical separation of the four channels, and complete wavelength coverage on each detector provides for high sensitivity and redundancy. The instrument also contains a fine error sensor to identify the pointing location and to stabilize the spacecraft during observations. Properties of the instrument are summarized in Table 5.

Table 6 contains pre-launch predictions for the in-orbit performance of FUSE. These quantities will be updated as in-orbit activities progress and astronomical observations are obtained. Figure 7 contains a plot of effective area at the beginning of the mission versus wavelength.

7. Launch and Operations

NASA will launch FUSE on a Delta II-7320 rocket into a 775 km circular, 25° inclination orbit in 1999 from the Cape Canaveral Air Station in Florida. During in-orbit checkout and early operations contact will be provided through a ground station in Hawaii. Once operational, the primary FUSE ground station at the University of Puerto Rico, Mayaguez will be used for most communications. Short duration (<13 minutes per orbit) S-band communications will occur 6–8 orbits per day, during which time data and commands will be sent between the spacecraft and the ground station. Communications between the

Table 5. Instrument Parameters

Mirrors (4):	Off-axis parabolas, zerodur substrate, 387×352 mm clear aperture
Gratings (4):	Spherical, aberration-corrected, holographically ruled, characteristic line densities of 5767 l/mm (SiC) and 5350 l/mm (LiF)
Optics Coatings:	SiC or Al+LiF
Detectors (2):	Microchannel plates with double delay-line anodes and KBr photocathodes
Spectrograph Design:	1.652 m Rowland circle
Instrument Size:	1.2 m × 1.8 m × 4.4 m
Instrument Mass:	780 kg

Table 6. FUSE Predicted Performance

Wavelength Coverage:	905–1187Å
Resolving Power:	$\lambda/\Delta\lambda \approx 24,000\text{--}30,000$
Effective Area:	20–80 cm ² (beginning of life)
Expected Degradation in A_{eff} :	$\sim 20\%$ yr ⁻¹
Science Apertures:	HIRS: (1.25''x20''), MDRS: (4''x20''), LWRS:(30''x30'')
Point Source Sensitivity:	
(MDRS aperture, S/N=10, R>24,000)	1 ksec at $F_{1030} = 1 \times 10^{-12}$ erg cm ⁻² s ⁻¹ Å ⁻¹ 10 ksec at $F_{1030} = 1 \times 10^{-13}$ erg cm ⁻² s ⁻¹ Å ⁻¹ 70 ksec at $F_{1030} = 2 \times 10^{-14}$ erg cm ⁻² s ⁻¹ Å ⁻¹
Bright Limit (point source):	$F_\lambda = 1 \times 10^{-10}$ erg cm ⁻² s ⁻¹ Å ⁻¹
Dark Limit (approximate):	$F_\lambda \sim 3 \times 10^{-15}$ erg cm ⁻² s ⁻¹ Å ⁻¹
Pointing Stability:	0.5'' in pitch and yaw (FES assisted)
Point Spread Function:	1.5'' (90% encircled energy)
FES Limiting Magnitude:	V \approx 15
FES Clear Field of View:	19' × 19'

ground station and the satellite control center on the Johns Hopkins University Homewood Campus will occur through an ISDN line. Observation planning, spacecraft instruction commanding, and pipeline reduction of scientific data will be performed in the FUSE Operations and Science Centers at Johns Hopkins. FUSE is the first mission of its kind to be developed and operated within a university setting.

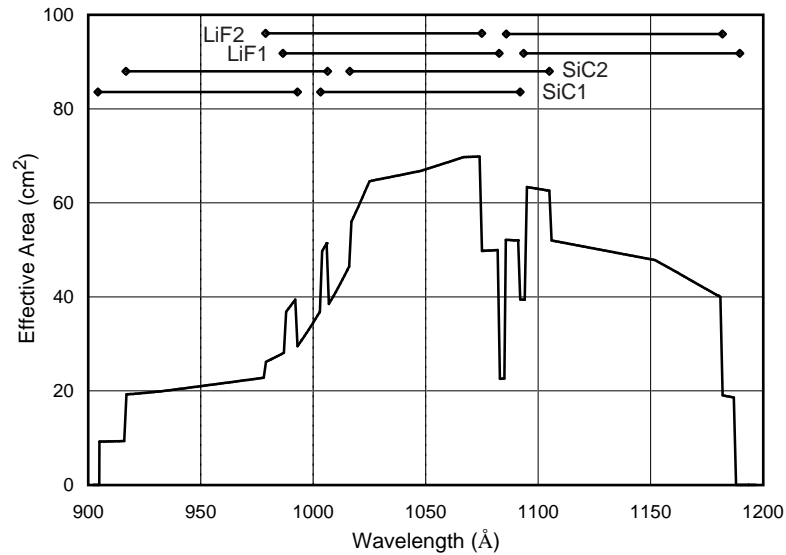


Figure 7. FUSE predicted effective area at the beginning of the mission. The individual detector segment coverages are indicated above the curve (4 segments - 2 SiC and 2 LiF per detector). The abrupt drops in effective area in some locations (e.g., 1082–1085Å) are due to gaps where the individual channels do not overlap completely.

8. Additional Information

Technical information about the initial performance results for FUSE have been given by Wilkinson *et al.* (1998) and Sahnou *et al.* (1998). Information about observing with FUSE can be found in the *FUSE Observer's Guide* (Oegerle *et al.* 1998) and on the FUSE web site at <http://fuse.pha.jhu.edu>. Guest Investigator questions can be directed to the GSFC FUSE Project Scientist, Dr. George Sonneborn, at sonneborn@stars.gsfc.nasa.gov.

Acknowledgments. It is a pleasure to thank the many dedicated people who are working so hard to make the FUSE mission happen. I thank Bill Oegerle and Ed Murphy for providing an initial version of the algorithm used to create Figures 5 and 6, and acknowledge useful conversations about H₂ and HD with Eric Burgh and Steve McCandliss.

References

- Abgrall, H., Roueff, E., Launay, F., Roncin, J.Y., & Subtil, J.L. 1993a, *A&AS*, 101, 273
- Abgrall, H., Roueff, E., Launay, F., Roncin, J.Y., & Subtil, J.L. 1993b, *A&AS*, 101, 323
- Allison, A.C. & Dalgarno, A. 1970, *Atomic Data*, 1, 289
- Anders, E. & Grevesse, N. 1989, *Geochim. Cosmochim. Acta*, 53, 197
- Dabrowski, I. & Herzberg, G. 1976, *Canadian Journal of Physics*, 54, 525
- Grevesse, N. & Noels, A. 1993, in *Origin of the Elements*, ed. N. Prantzos, E. Vangioni-Flam, & M. Cassé, (Cambridge: Cambridge University Press), 15
- Harris, A.W. & Bromage, G.E. 1984, *MNRAS*, 208, 941
- Jenkins, E.B. 1987, in *Interstellar Processes*, eds. D.J. Hollenbach & H.A. Thronson, (Dordrecht: Reidel), 533

- Jenkins, E.B. 1996, ApJ, 471, 292
- Jenkins, E.B., Savage, B.D., & Spitzer, L. 1986, ApJ, 301, 355
- Jura, M. 1974, ApJ, 191, 375
- Jura, M. & York, D.G. 1978, ApJ, 219, 861
- Linsky, J.L., Brown, A., Gayley, K., Diplas, A., Savage, B.D., *et al.* 1993, ApJ, 402, 694
- Lu, L., Savage, B.D., Sembach, K.R., Wakker, B.P., Sargent, W.L.W., & Oosterloo, T.A. 1998, AJ, 115, 162
- Meyer, D.M., Jura, M., & Cardelli, J.A. 1998, ApJ, 493, 222
- Moore, C.E. 1970, *Ionization Potentials and Ionization Limits Derived from the Analysis of Optical Spectra*, Rep. No. NSRDS-NBS34 (Washington, D.C.: US Department of Commerce)
- Morton, D.C. 1991, ApJS, 77, 119
- Morton, D.C. & Noreau, L. 1994, ApJS, 95, 301
- Sahnow, D.J., Friedman, S.D., Moos, H.W., Green, J.C., & Siegmund, O.H.W. 1998, Proc. SPIE, 3356, 552
- Oegerle, W.R., Murphy, E.M., Blair, W.P., Kriss, G.A., & Friedman, S.D. 1998, *The FUSE Observer's Guide, v1.2* (<http://fuse.pha.jhu.edu>)
- Savage, B.D. & Sembach, K.R. 1991, ApJ, 379, 245
- Savage, B.D. & Sembach, K.R. 1996, ARA&A, 34, 279
- Sembach, K.R., Savage, B.D., Lu, L., & Murphy, E.M. 1995, ApJ, 451, 616
- Sembach, K.R., Savage, B.D., Lu, L., & Murphy, E.M. 1999, ApJ, 515 (April 10)
- Spitzer, L. 1978, *Physical Processes in the Interstellar Medium*, (New York: John Wiley & Sons)
- Sutherland, R.S. & Dopita, M.A. 1993, ApJS, 88, 253
- Tufte, S.L., Reynolds, R.J., & Haffner, L.M. 1998, ApJ, 504, 773
- Wakker, B.P., Murphy, E.M., van Woerden, H., & Dame, T.M. 1997, ApJ, 488, 216
- Wakker, B.P. & van Woerden, H. 1997, ARA&A, 35, 217
- Wilkinson, E., Green, J.C., Osterman, S.N., Brownsberger, K.R., & Sahnow, D.J. 1998, Proc. SPIE, 3356, 18
- Wright, E.L. & Morton, D.C. 1979, ApJ, 227, 483